RESEARCH ARTICLE OPEN ACCESS

Inductive sensor and its drive circuit development

Chia-Juei Fan[1], Wei-Tao Huang[2], Chao-Yun Chen[3*]
Green Energy and Environment Research Laboratories, Industrial Technology Research Institute, Chutung, Hsinchu, Taiwan
Email: [1]CJFan@itri.org.tw, [2]WTHuang@itri.org.tw, [3*]cychen1022@itri.org.tw

Abstract:

This study is concerned with the displacement detection of the noncontact rotated object. In the commercially sensor modules for the noncontact detection applications, its modules included the sensor probe and power amplimer/drive circuit, however, these sensor modules are very expensive and poor applicability. Therefore, this study develops a sensor module with the high cost-performance ratio, in which the sensor probe is aim at the inductive type, which mathematical model, sensor probe implementation, sensor probe test and analysis, and applied operation principle will be presented fully. Moreover, this study integrated the resonant circuit, filter and rectifier to proposed a drive circuit of the sensor probe, the drive circuit can output the DC voltage of the displacement for the various control applications. Finally, the experimental result shows the sensitivity and linearity of the inductive sensor probe integrated with the proposed drive circuit.

Keywords —**Inductive sensor, drive circuit, sensitivity, linearity**

I. INTRODUCTION

In the industrial applications, the displacement, velocity, and vibration detection of the mechanism is the crucial issues, such as the displacement detection of the rotor in the maglev compressor, because the rotor is supported by the active magnetic bearing, which advantages concluded the noncontact, oil-free, and controllability, in which the control performance of the rotor positioning is based on the accuracy of the position feedback signal, and it is inevitable that the position signal quality must depend on the sensor module [1].

In the literature review of the contactless sensor, Kejık etal. [2] proposed compact hybrid inductive sensor that is composed of a sensing flat coil and an integrated electronic interface, which benefit is the low cost for industrial applications, but its flat coil structure is not suitable for the displacement detection of the rotated object. Wang etal. [3] proposed an inductive sensor probe to detect the metal abrasive particles of mechanical transmission systems, which specific application design is the saddle-coil that is more difficult to apply to the rotating machinery. Zhao etal. [4] applied the inductive sensor to develop a high temperature-resistant inductive sensor for blade tip clearance measurement of the aero-engine, which experimental results have shown the sensor resolution and sensing range, and the temperature effects are also obtained. Ripka etal. [5] have shown the inductive position sensor development in their laboratories for industrial application, and presented the high precision performance for the large working distance and large resistance to the environmental conditions. Liu etal. [6] applied the circuit topology approach to develop the eddy current sensor and proposed a method that provides additional parameters as capacitance value in characterizing both winding capacitance and coaxial cable capacitance and resistance value characterizing conductivity variations due to crack or stress. Babu etal. [7] proposed a noncontact, planar spiral coil-based displacement sensor, its characteristics included the planar coil and the movable U-shaped magnetic core, and the sensor performance exhibited the high qualities for measurement error and resolution. Xu etal. [8] proposed an eddy current sensor using the Colpitts circuit with the characteristics of long measurement range and better linearity, and the linearity can be reduced to within ± 0.4%, the sensitivity is

0.28V/mm. Wang etal. [9] proposed a novel displacement probe using PC magnetizers and TMR sensors, in which the probe design is based on the magnetic flux measurement principle and the PC magnetizer can generate a uniform magnetization field distribution, while the TMR sensor detect the magnetic field and the distance from the ferromagnetic material can be obtained. Gao etal. [10] presented a planar PCB-type displacement sensor using the eddy current principle, the ability of this sensor is based on the coil design and software-tuning parameters to achieve the contactless measurement.

In the commercially sensor module products, the cost is not conductive to productization, the sensor structure is difficult to customize to the practical applications, and more importantly, the sensor performance cannot meet the requirements of the high-speed contactless rotated rotor. Although many research literatures have presented the great performance of the contactless sensor, however their coil design is the planar PCB type, this structure is not suitable for the applications of rotating machinery and increasing the difficulty of institutional matching. Furthermore, the drive circuit is the most critical point of sensing performance, such as the linearity and sensitivity. Because the engineering tolerance caused by the machining and assembly, the engineering tolerance will affect the sensing performance that must be adjusted through the elements on the drive circuit, and easily implementation and tuning intuitive are the key factor in the industrial applications. In view of this, this study proposes a noncontact inductive sensor module that included the sensor probe and the drive circuit, in which the sensor probe adopts a dual coil probe type which material is the silicon steel sheet, and the winding is the series dual coil, in order to enhance magnetic field, the sensing area of the object is designed with the silicon steel sheet stack. Moreover, the drive circuit is based on the resonant principle to adopt the filter and rectifier algorithms. Additionally, linearity and sensitivity have been considered for easily implementation and tuning intuitive in the practical applications, this study proposes the replaceable capacitance and resistance of the drive circuit, in which the replaceable capacitance can adjust the resonant frequency that will determine the performance both linearity and sensitivity, and the replaceable resistance can adjust the DC voltage range that is used as the displacement signal in practical applications. Finally, a micro-motion platform is used to verify the proposed sensor module, and the experimental results show the satisfactory performance.

The rest of this paper is organized as follows. Section II gives the inductive sensor probe implementation. Section III shows the drive circuit design of sensor probe. Experimental setup and results are included in Section IV, while conclusions are drawn in Section V.

II. Inductive Sensor Model and Simulations

A. The modelling of the inductive sensor probe

The basic operation principle of the inductive sensor is based on the inductance variations between the sensor probe and object, and produces the DC voltage using the drive circuit. Fig. 1 shows the sensing diagram, in which the silicon steel sheet laminations and coils are the structure design of sensor probe. According to the principle of the electromagnetic induction [10], the coil passes a specified current to generate the magnetic field, and the magnetic circuit can be determined through the geometric design of the silicon steel sheet laminations. The mutual inductance changes with the variation of displacement x. Therefore, the inductance variation measurement that can determine the magnitude and direction of the sensing object displacement.

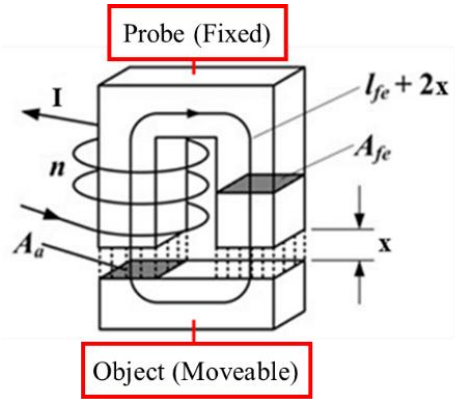

Fig. 1. The sensing diagram between probe and object.

This study is based on the magnetic field definition to derive the model of the inductive sensor, the relational expression between the inductance L and current I can be written as

$$n\Phi_m = LI \quad (1)$$

where Φ_m is the total flux generated by the coil turns N. The magnetomotive force F_m can be shown as

$$F_m = nI \quad (2)$$

and the flux Φ_m can be expressed as m

$$\Phi_m = \frac{F_m}{R_m} \quad (3)$$

Substituting Eqs. (2) and (3) into Eq. (1) can be obtained as

$$L = \frac{n^2}{R_m} \quad (4)$$

According to the Fig. 1, the total magnetoresistance can be written as

$$R_m = \frac{l_{fe}}{\mu_{fe}A_{fe}} + \frac{2x}{\mu_0 A_a} \quad (5)$$

where l_{fe} is the length of magnetic circuit, μ_{fe} is the relative magnetic permeability between the probe and object, A_{fe} is the cross-section area of probe, x is the air gap, μ_0 is the vacuum permeability, A_a is the cross-section area of air gap. Substituting Eq. (5) into Eq. (4) can derive the expression of L and x,

$$L = \frac{n^2}{\frac{l_{fe}}{\mu_{fe}A_{fe}} + \frac{2x}{\mu_0 A_a}} \quad (6)$$

Assuming that the air gap is large, the magnetic resistance of air is much greater than the magnetic resistance of silicon steel sheets, Therefore, the magnetic resistance of the silicon steel sheet can be ignored, Eq. (6) can be simplified to the following formula.

$$L = \frac{n^2\mu_0 A_a}{2x} \quad (7)$$

B. The sensor probe implementation

The model of 3D sensor probe drawing is shown as Fig. 2, and the relationship between displacement and inductance can be shown in Fig. 3, where the blue curve is obtained through analytical solution using Eq. (7) and the red curve is obtained through the commercial software, the trends of the two curves are almost the same when the air gap is very large, but the inductance of the model analytical solution will rise sharply when the air gap is very small. Exploring the reasons for this difference, Eq. (7) has ignored the magnetic resistance of the silicon steel sheet under the small displacement. For this consideration, the revised analyze results is shown in Fig. 4, the inductance value of the red curve still has difference compared with the blue curve under the small displacement, because of the Eq. (6) and Eq. (7) are the simplified mathematical model that ignored many practical conditions.

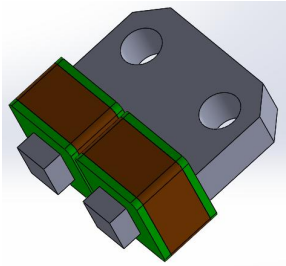

Fig. 2. The 3D diagram of sensor probe

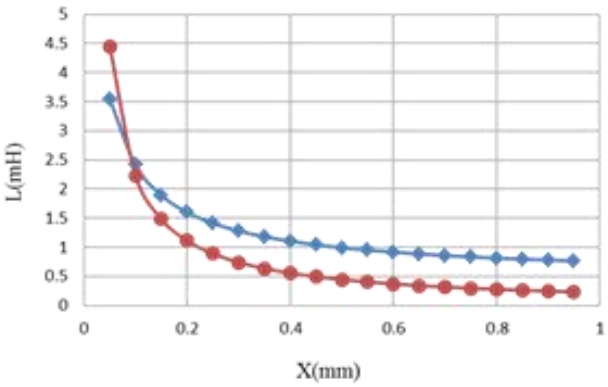

Fig. 3. The relationship between displacement and inductance

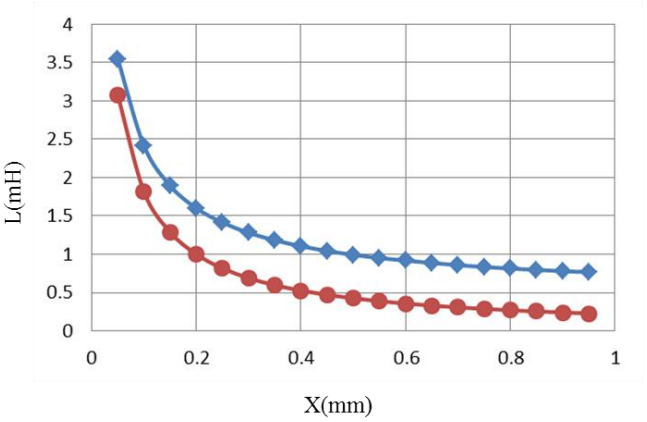

Fig. 4. The revised relationship between displacement and inductance

In order to implement the design of Fig. 2 and verify the sensor probe characteristics under the different excitation frequency, this study completed

12 test sensor probes, which the design values of the resistance and inductance are 2.4Ω and 500μH respectively, the practical sensor probe is shown in Fig. 5.

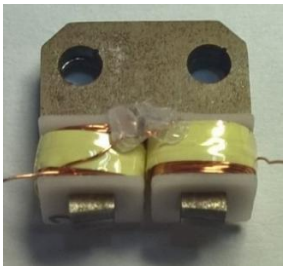

Fig. 5. A practical sensor probe sample.

The measured values of the resistance and inductance for the 12-test sensor probe are shown in Table 1, where R is the measured resistance, E_R is the error between the 2.4Ω and R, L is the measured inductance, and E_L is the error between 500μH the and L.

Table 1. The measured values of the 12 test sensor probe

Number	R (Ω)	E_R %	L (μH)	E_L %
01	2.389	-0.541	513.5	1.450
02	2.385	-0.708	511.1	0.976
03	2.442	1.665	508.4	0.443
04	2.409	0.291	503.1	-0.605
05	2.410	0.333	515.8	1.905
06	2.413	0.458	501.7	-0.881
07	2.379	-0.958	507.9	0.344
08	2.408	0.249	502.6	-0.703
09	2.400	-0.083	497.0	-1.810
10	2.388	-0.583	513.9	1.529
11	2.415	0.541	511.4	1.035
12	2.386	-0.666	487.5	-3.687

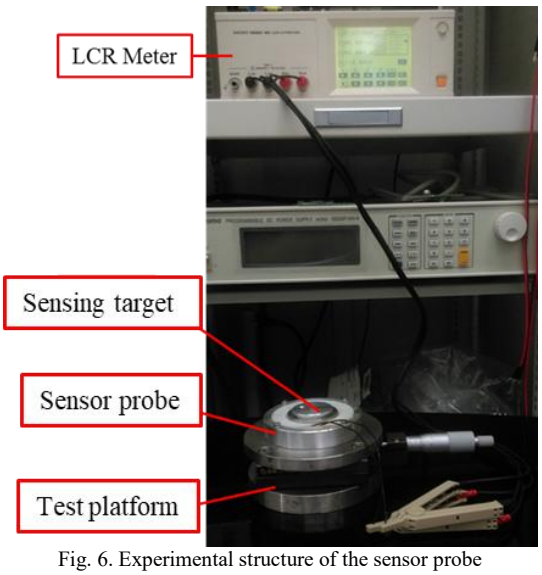

Fig. 6. Experimental structure of the sensor probe

Fig. 6 is the experimental structure diagram of the sensor probe characteristic measurement, where the LCR meter is used to measure the inductance using the different excitation frequency and the various displacements. The experimental results have shown in Fig. 7, which results indicate that characteristic curve of the different excitation frequency. The inductance variations will decrease when the frequency increases, this situation will result in the poor sensitivity. However, the low-frequency (10Hz) characteristic curve is almost consistent with the model analytical solution. The conclusion is that the current mathematical model does not take frequency into consideration and can only describe the phenomenon of static magnetic fields.

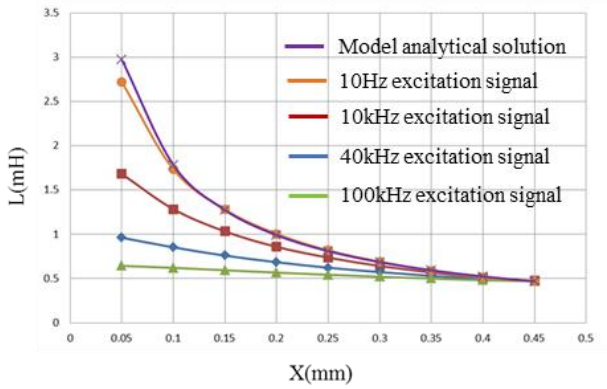

Fig. 7. The experimental results of the sensor probe characteristic.

III. DRIVE CIRCUIT OF THE INDUCTIVE SENSOR

The operating principle of the drive circuit is shown in Fig. 8, the inductive sensor can be regarded as an inductance, the operation process is described as follows. First, an excitation signal is input to the probe coils through the RLC resonant circuit, the area between sensor probe and ferromagnetic object will generate an induced magnetic field, which strength changes with the distance between sensor probe and ferromagnetic object, and this strength of the induced magnetic causes the variations of the induced voltage through the resonant circuit, which means that the mutual inductance will also change accordingly. Second,

the induced voltage signal transfers to DC voltage using the filter and rectifier circuit.

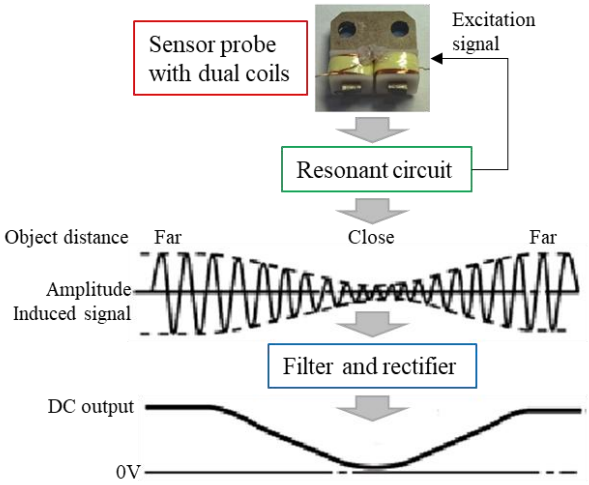

Fig. 8. The operating principle of the drive circuit

There are two crucial points of derive circuit are to guarantee the performance of the sensor module. The principle diagram of the sensitivity tuning is shown in Fig. 9, the resonant circuit is based on the RLC resonant theory, and the design of the sensor probe has decided the resistance *R* and inductance *L*, the maximum sensitivity represents the maximum voltage amplitude when the operation frequency of RLC circuit is located on the resonant point.

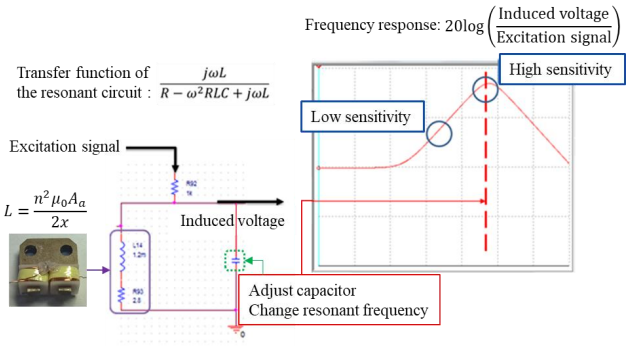

Fig. 9. The principle diagram of the sensitivity tuning.

Fig. 10 shows the linearity tuning of the inductive sensor module, because of the corresponding relationship between the displacement x and inductance L have been decided by the magnetic circuit design of sensor probe, and the capacitance of RLC resonant circuit determines corresponding relationship between the displacement voltage Vout and the inductance L. However, the L-x curve and the Vout-x curve are both nonlinear, and presents the inverse curves with each other. Therefore, the linearity between the displacement and output voltage can theoretically be adjusted through the capacitance.

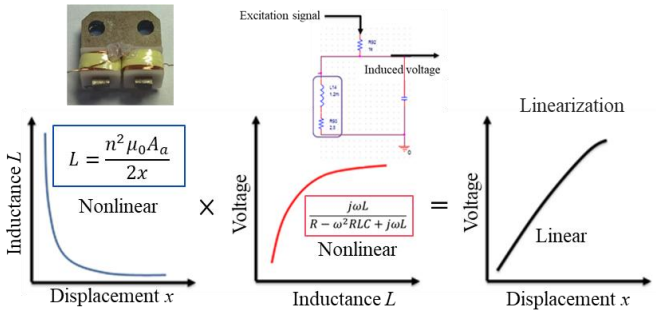

Fig. 10. The principle diagram of the linearity tuning.

According to the above descriptions of sensitivity and linearity, the drive circuit design can be shown in Fig. 11, where the part A is the power circuit, part B is the RLC resonant circuit, and part C is the rectifier circuit. Considering the part B, the dual sensor probes are used as the differential type for simulating the rotor displacement measurement, L3 and R6 are one sensor probe, L4 and R4 are another sensor probe, and a variable inductor is set on each of the two sensor probes, the variable inductor is simulated to the rotor displacement, because the inductance changes with the displacement (Fig. 7), and the excitation signal of the dual sensor probes is the square wave, which frequency is 40kHz.

The differential schematic diagram of rotor displacement measurement is shown in the Fig. 12. when the rotor is positioned in the center, the output DC voltage of drive circuit is 2.49V, that is the rotor positioning center, which simulation results is shown in Fig. 13, which indicates that the induced voltages from both sensor probes have overlapped and the inductance variations of the two sensor probes are the same. Moreover, when the rotor undergoes *x* displacement and the rotor is close to the probe 2, which can be shown in Fig. 14, the induced voltages of the probe 2 is bigger than the induced voltages of the probe 1, the output voltage is 99.62 mV, the simulation result can be shown in Fig. 15. Otherwise, when the rotor is close to the probe 1, which can be shown in Fig. 16, the induced voltages of the probe 1 is bigger than the induced

voltages of the probe 2, the output voltage is 4.9V,
the simulation result can be shown in Fig. 17.

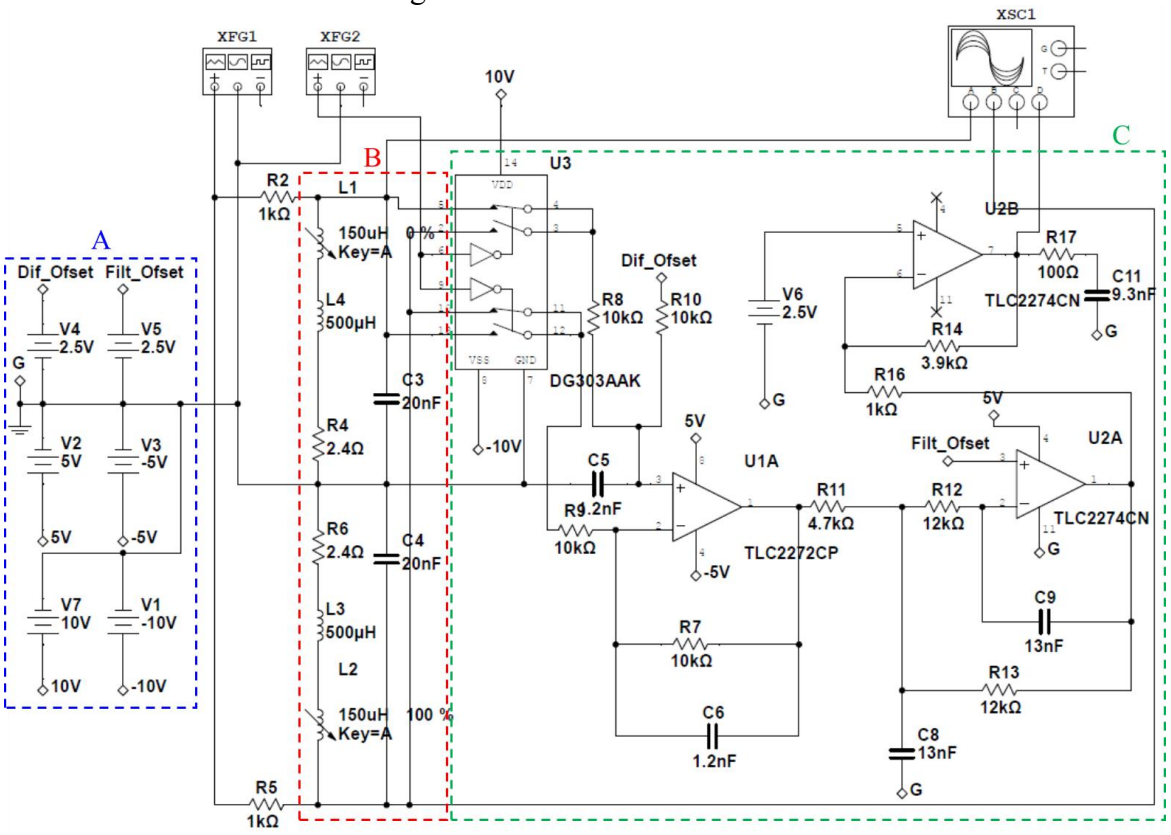

Fig. 11. The drive circuit of the inductive sensor probe.

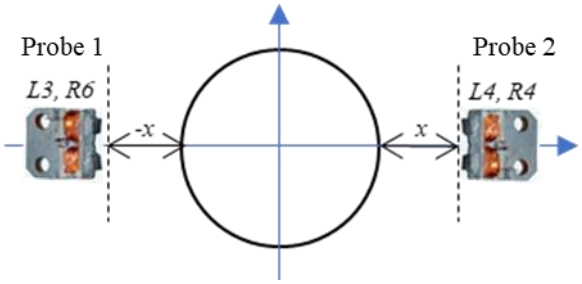

Fig. 12. The differential type of the dual sensor probes in the rotor displacement.

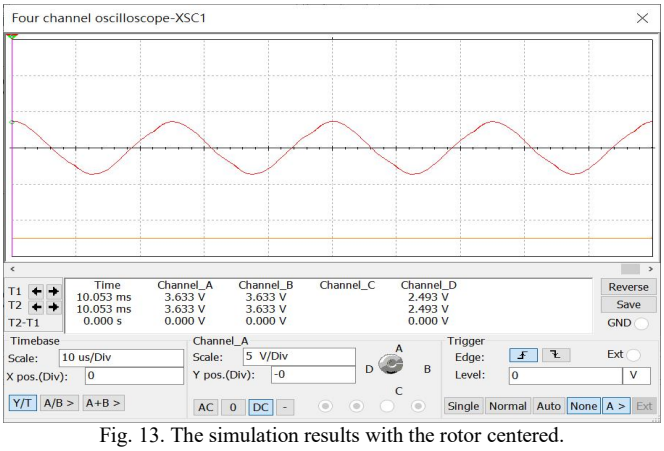

Fig. 13. The simulation results with the rotor centered.

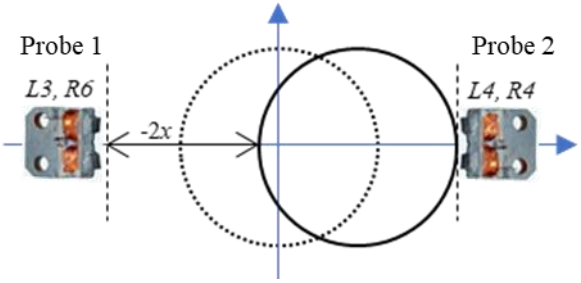

Fig. 14. The differential type of the dual sensor probes with rotor is close to probe 2.

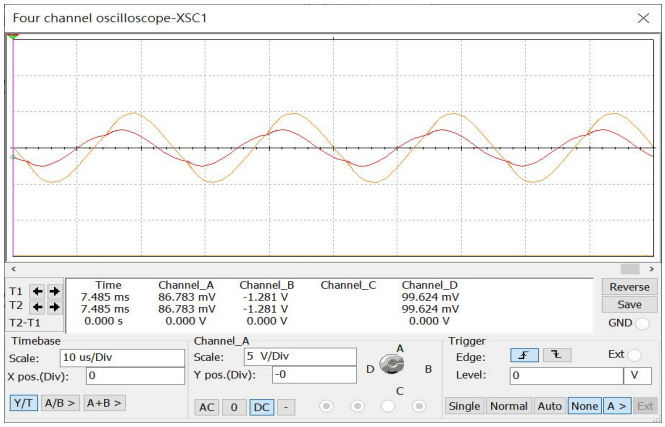

Fig. 15. The simulation results with the rotor is close to probe 2.

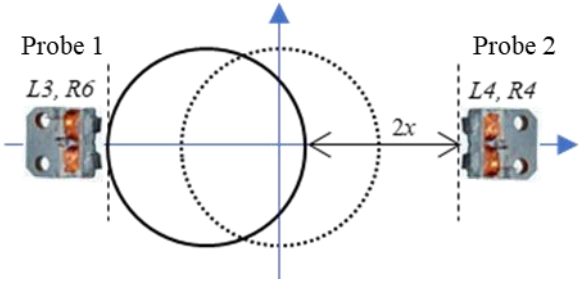

Fig. 16. The differential type of the dual sensor probes with rotor is close to probe 1.

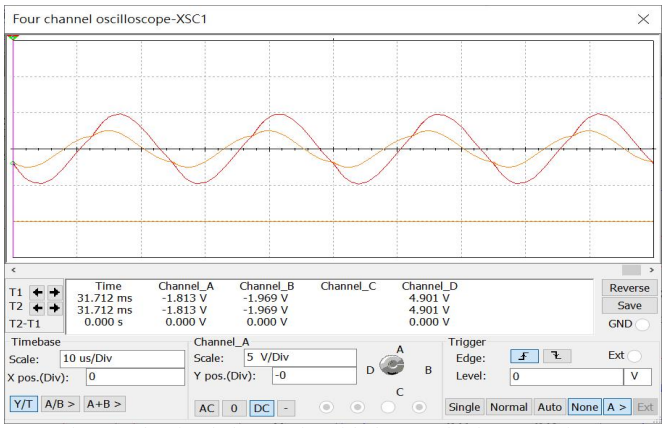

Fig. 17. The simulation results with the rotor is close to probe 1.

IV. EPERIMENTAL RESULTS OF THE SENSOR MODULE PERFORMANCE

This section presents the experimental results of the sensor module performance that included the linearity and the sensitivity.

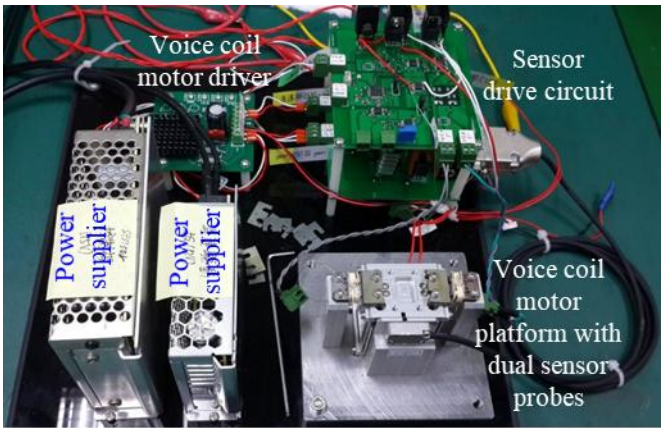

Fig. 18. The experiment platform of the sensor module performance test.

Fig. 18 has shown the experiment platform that included voice coil motor platform with dual sensor probes, sensor drive circuit, voice coil motor driver, and power suppliers. The voice coil motor platform has equipped with the optical linear encoder that is used to detect the displacement, and the dual sensor probes configuration are the differential type, and the movement range of the voice coil motor platform is set to 100 μm that is used to verify the linearity and the sensitivity.

The experimental results are shown in Fig. 19. From the results can be obtained that the linearity is F.S. 0.36% (Full Scale) and the sensitivity is 10mV.

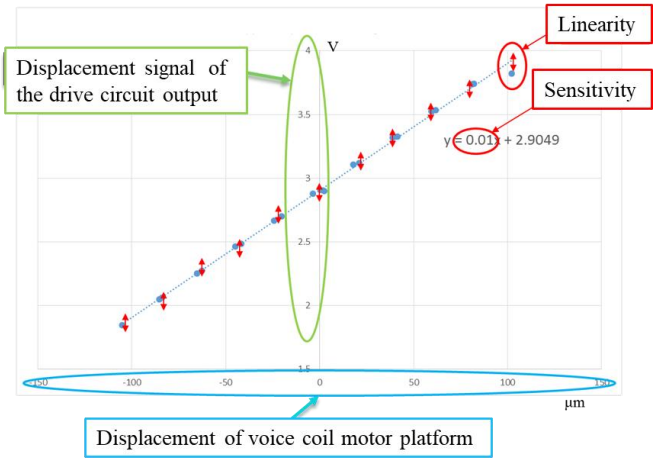

Fig. 19. The experimental results of the differential sensor module.

V. CONCLUSIONS

This study presents the inductive sensor and sensor drive circuit development. First, the sensor

probe adopts the dual coil type, and the inductance error and resistance error of the 12 sensor probes are less than 2%. Second, the drive circuit is developed for the sensor probe performance verification, and the tuning principle of the sensor module has been presented. Third, the experimental results have shown the linearity and sensitivity, the linearity is F.S. 0.36% and the sensitivity is 10mV. Finally, the results of this study present the inductive sensor module with the high cost/performance ratio that is very suitable for the various industrial applications that included the displacement, vibration and speed measurement.

ACKNOWLEDGMENT

The author would like to thank the Energy Administration, Ministry of Economic Affairs, Taiwan, R.O.C., for supporting this research.

REFERENCES

[1] G. Schweitzer and E. H. Maslen, Magnetic bearing, Springer-Verlag Ber. Heidelberg, 2009.

[2] P. Kejik, C. Kluser, R. Bischofberger, and R. S. Popovic, “A low-cost inductive proximity sensor for industrial applications,” *Sensors and Actuators A*, vol. 110, no. 1-3, pp. 93-97, Feb. 2004.

[3] C. wang, X. Liu, and Z. Chen, “Probe improvement of inductive sensor for online health monitoring of mechanical transmission system,” *IEEE Transactions on magnetics*, vol. 51, no. 11, 4004404, Nov. 2015.

[4] Z. Zhao, Z. Liu, Y. Lyu, and Y. Gao, “Experimental investigation of high temperature-resistant inductive sensor for blade tip clearance measurement,” *Sensors*, vol. 19, no. 1, pp. 1-13, Dec. 2018.

[5] P. Ripka, J. Blazek M. Mirzaei, P. Lipovsky, M. Smelko, and K. Draganova, “Inductive position and speed sensors,” *Sensors*, vol. 20, pp. 65-77, Dec. 2019.

[6] D. Liu, H. Zhang, X. Xiao, Q. Ma, H. Li, G. Tian, B. Gao, and J. Wu, “RLC parameters measurement and fusion for high-sensitivity inductive sensors,” *IEEE transactions on instrumentation and measurement*, vol. 71, pp. 11617 – 11624, May 2022.

[7] A. Babu and B. George, “Design and development of a new non-contact inductive displacement sensor,” *IEEE sensors journal*, vol. 18, no. 3, pp. 976-984, Feb. 2018.

[8] C. Xu, S. Yu, and M. Liu, “Design and analysis of an eddy current displacement sensor with extended linear range,” *Sensor and actuators: A. physical*, vol. 368, pp. 115100-115110, Apr. 2024.

[9] S. Wand, B. Feng, Y. Hu, G. Qiu, Z. Duan, and Y. Kang, “Displacement meqasurement for ferromagnetic materials based on the double-layer parallel-cable-based probe,” *Sensors and actuators: A.* physical, vol. 362, pp. 114599-114608, 2023.

[10] W. Gao, H. Shi, and Q. Tang, “A contactless planar inductive sensor for absolute angular displacement measurement,” IEEE access, vol. 9, pp. 160878-160886, Nov. 2021.

[11] S. J. Chapman, Electric Machinery Fundamentals, New York, NY, USA:McGraw-Hill, 2012.